Available online at www.sciencedirect.com
ScienceDirect
Coordination Chemistry Reviews 250 (2006) 2335–2346
COORDINATION CHEMISTRY REVIEWS
www.elsevier.com/locate/ccr

Review

Tuning of electronic structures of quasi one-dimensional iodide-bridged dinuclear platinum mixed-valence complexes

Masahiro Yamashita [a,*], Shinya Takaishi [a], Atsushi Kobayashi [b], Hiroshi Kitagawa [b,*], Hiroyuki Matsuzaki [c], Hiroshi Okamoto [c,*]

[a] *Graduate School of Science, Tohoku University & CREST(JST), Aoba-ku, Sendai 980-8578, Japan*
[b] *Department of Chemistry, Faculty of Science, Kyushu University, Higashi-ku, Fukuoka 812-8581, Japan*
[c] *Graduate School of Frontier Science, The University of Tokyo, Kashiwanoha, Kashiwa, Chiba 277-8561, Japan*

Received 26 January 2006; received in revised form 3 March 2006; accepted 9 March 2006
Available online 17 March 2006

Contents

Abstract

This review describes the tuning of electronic structures and variable phase transitions in quasi one-dimensional iodide-bridged dinuclear Pt compounds (MMX chains). These are classified into two types of MMX chain compounds, that is, $Pt_2(dta)_4I$ (dta = dithioacetate derivatives) and $R_4[Pt_2(pop)_4I]\cdot nH_2O$ (R = alkylammonium, etc.; pop = $P_2O_5H_2^{2-}$). These MMX chains compounds can take four electronic structures such as average valence (AV), charge-density-wave (CDW), charge-polarization (CP) and alternating charge-polarization (ACP) states. The $Pt_2(dta)_4I$ compounds show a phase transition from metallic AV, CP, to ACP state with decreasing temperature. The phase transition feature depends on the alkyl derivatives of the dta ligands. The $R_4[Pt_2(pop)_4I]\cdot nH_2O$ exhibits three oxidation states, AV, CDW, and CP states, depending on the kind of cations. Some of these compounds show a phase transition by pressure, photo-irradiation, temperature, and humidity.

Keywords: Phase transition; Photo-irradiation; MMX chain compounds

1. Introduction

The search for high-temperature superconductivity and novel superconducting mechanisms is one of the most challenging tasks of condensed-matter physicists and materials research scientists. Bednorz and Müller considered the mixed-valence effect of Cu ions in the $La_{1-X}Ba_XCuO_4$ system as a mechanism for strong electron–phonon interactions allowing a high T_c. We are interested in the possibility of an unusual superconducting state, which results from the condensation of bipolarons, and is postulated under a strongly coupled electron–phonon system [1]. According to this model, Cooper-pair formation due to the condensation of bipolarons occurs under some electron–phonon coupling constant λ, while in the large λ limit bipolaron formation occurs in real space.

Quasi one-dimensional (1D) halogen-bridged mononuclear Pt and Pd compounds (MX chains) are regarded as an on-site bipolaronic state where bipolarons form a 1D lattice and localize at M^{II} sites; it has been investigated as "a model material" to search for high T_c values. To date, many attractive physi-

* Corresponding authors.
E-mail addresses: yamasita@agnus.chem.tohoku.ac.jp (M. Yamashita), hiroshiscc@mbox.nc.kyushu-u.ac.jp (H. Kitagawa), okamotoh@k.u-tokyo.ac.jp (H. Okamoto).

0010-8545/$ – see front matter © 2006 Elsevier B.V. All rights reserved.
doi:10.1016/j.ccr.2006.03.006

cal properties based on the electron–phonon interaction have been observed such as intense and dichroic intervalence charge transfer bands, overtone progressions of resonance Raman spectra, luminescence spectra with large Stokes-shifts, and midgap absorption attributable to solitons and polarons [2–6] On the other hand, halogen-bridged Ni compounds have also been attractive targets because they show interesting physical properties owing to their electronic correlation, e.g. a quite strong antiferromagnetic interaction [7], a spin-Peierls transition [8] and a gigantic third-order non-linear optical susceptibility [9]. Recently, increasing attention has been focused on a wide variety of 1D electronic states of chain compounds composed of dinuclear M–M units as an alternative model material. In these compounds, two metal ions are linked by four ligands to form a lantern structure $[M_2(L–L)_4]$ [10–18], and the neighboring lantern units are bridged by halide ions (X), forming a linear chain structure with the ···M–M–X··· repeating units. Therefore, these compounds are abbreviated as MMX chains. In the MMX chain compounds, four electronic structures are possible depending on the positions of the bridging halogen ions as follows:

(1) $–X–Pt^{2.5+}–Pt^{2.5+}–X–Pt^{2.5+}–Pt^{2.5+}–$ (=averaged-valence (AV) state).
(2) $\cdots X–Pt^{3+}–Pt^{3+}–X\cdots Pt^{2+}–Pt^{2+}\cdots$ (=charge-density-wave (CDW) state).
(3) $\cdots X–Pt^{3+}–Pt^{2+}\cdots X–Pt^{3+}–Pt^{2+}\cdots$ (=charge-polarization (CP) state).
(4) $\cdots X\cdots Pt^{2+}–Pt^{3+}–X–Pt^{3+}–Pt^{2+}\cdots$ (=alternating charge-polarization (ACP) state).

So far, two types of MMX chain compounds have been reported. One is $[M_2(dta)_4I]$ (M = Pt and Ni; dta = $C_nH_{2n+1}CS_2^-$, n = 1–4), which form neutral chains [10,11,19–30]. Another is $R_4[Pt_2(pop)_4X]\cdot nH_2O$ (R = alkylammonium ions, alkyldiammonium ions, alkali metal ions: X = Cl, Br and I), which form anionic chains [14,15,31,32]. Because platinum ions usually have a larger hybridization with iodides than chloride and bromides, iodide-bridged compounds are expected to stabilize the various oxidation states and, as a result, cause the various phase transitions.

In this review, we will describe the tuning of electronic structures and phase transitions in quasi-one-dimensional iodide-bridged dinuclear platinum compounds.

2. Tuning of electronic structures of $R_4[Pt_2(pop)_4I]\cdot nH_2O$ and $R'_2[Pt_2(pop)_4I]\cdot nH_2O$

Starting materials, $K_4[Pt_2^{2+}(pop)_4]$ and $K_4[Pt_2^{3+}(pop)_4I_2]$ were synthesized by the methods reported previously. The quasi-one-dimensional iodide-bridged dinuclear Pt complexes, $R_4[Pt_2(pop)_4I]\cdot nH_2O$ and $R'_2[Pt_2(pop)_4I]\cdot nH_2O$ were synthesized by mixing equimolar aqueous solutions of $K_4[Pt_2^{2+}(pop)_4]$ and $K_4[Pt_2^{3+}(pop)_4I_2]$ followed by addition of excess amounts of alkylammonium (R) nitrate or alkyldiammonium (R′) nitrate.

Fig. 1 shows the structures of $[NH_3(C_6H_{12})NH_3]_2[Pt_2(pop)_4I]$ and $[(C_2H_5)_2NH_2]_4[Pt_2(pop)_4I]$. In both compounds, two Pt ions are linked by four pop ligands to form lantern structures $[Pt_2(pop)_4]$. The neighboring $[Pt_2(pop)_4]$ units are bridged by iodide ions, forming a linear chain Pt–Pt–I structure. The bridging iodide ions are disordered at the displaced position from the midpoints between the neighboring dinuclear Pt units with half occupancies, indicating that the electronic states of these compounds are the CDW or CP states. It is quite difficult to determine whether these compounds are in the CDW or CP states by conventional X-ray crystal structure analysis because displacements of the bridging iodide ions are disordered. In both compounds, the counter cations are located in the interchain spaces. Hydrogen bonds between the ammonium protons and oxygen atoms of the pop ligands exist, which stabilize the Pt–Pt–I linear chain structures.

Inter-valence charge transfer (CT) bands should reflect the electronic states of the compounds, namely the CT band in the CP state should be observed within the Pt dimer units ($Pt^{2+} \rightarrow Pt^{3+}$), while that in the CDW state should be observed between the dimer unites ($Pt^{2+} \rightarrow Pt^{3+}$). Fig. 2 shows the optical conductivity spectra obtained by Kramers-Kronig transformation of the single-crystal reflectance spectra in $[NH_3(C_6H_{12})NH_3]_2[Pt_2(pop)_4I]$ and $[(C_2H_5)_2NH_2]_4[Pt_2(pop)_4I]$. Optical gap energies ($E_{CT}$) differ considerably, namely E_{CT} of the former and the latter compounds are 2.4 and 1.0 eV, respectively.

Resonant Raman spectroscopy is a useful method to determine the electronic states of these compounds, because the CP and CDW states show different Pt–Pt stretching modes ν(Pt–Pt), namely ν(Pt–Pt) in the CP and CDW states should be a singlet (Pt^{2+}–Pt^{3+}) and doublet (Pt^{2+}–Pt^{2+} and Pt^{3+}–Pt^{3+}), respectively. The Raman spectra of the present compounds are shown in Fig. 3. Strong bands at 80–100 cm^{-1} are attributed to the Pt–Pt stretching modes of the dinuclear Pt units. In $[NH_3(C_6H_{12})NH_3]_2[Pt_2(pop)_4I]$, a doublet signal (85 and 95 cm^{-1}) of the dinuclear Pt–Pt units is observed, which is reasonably assigned to the $\nu(Pt^{2+}–Pt^{2+})$ and $\nu(Pt^{3+}–Pt^{3+})$, suggesting that $[NH_3(C_6H_{12})NH_3]_2[Pt_2(pop)_4I]$ is in the CDW state. On the other hand, in $[(C_2H_5)_2NH_2]_4[Pt_2(pop)_4I]$, a singlet signal at 98 cm^{-1} is observed, which is assigned to $\nu(Pt^{2+}–Pt^{3+})$, indicating that the $[(C_2H_5)_2NH_2]_4[Pt_2(pop)_4I]$ is in the CP state. The weak bands around 110 cm^{-1} can be attributed to the Pt–I stretching mode, which is activated by displacements of iodide ions in both compounds.

The compounds in the CP state are composed of Pt^{2+}–Pt^{3+} paramagnetic units (the Pt^{3+} ion have a spin 1/2), forming a one-dimensional spin chain, while those in the CDW state are composed of Pt^{2+}–Pt^{2+} and Pt^{3+}–Pt^{3+} diamagnetic units because the two neighboring Pt^{3+} ions form a spin singlet. Therefore, the magnetic properties should be influenced by the electronic state of the compounds. The temperature dependence of χ_{spin} is presented in Fig. 4. In the $[NH_3(C_6H_{12})NH_3]_2[Pt_2(pop)_4I]$, the χ_{spin} follows the Curie law as shown by the broken line in Fig. 4. Spin concentration is evaluated to be 0.16% per Pt site. Therefore, these paramagnetic spins should have an extrinsic

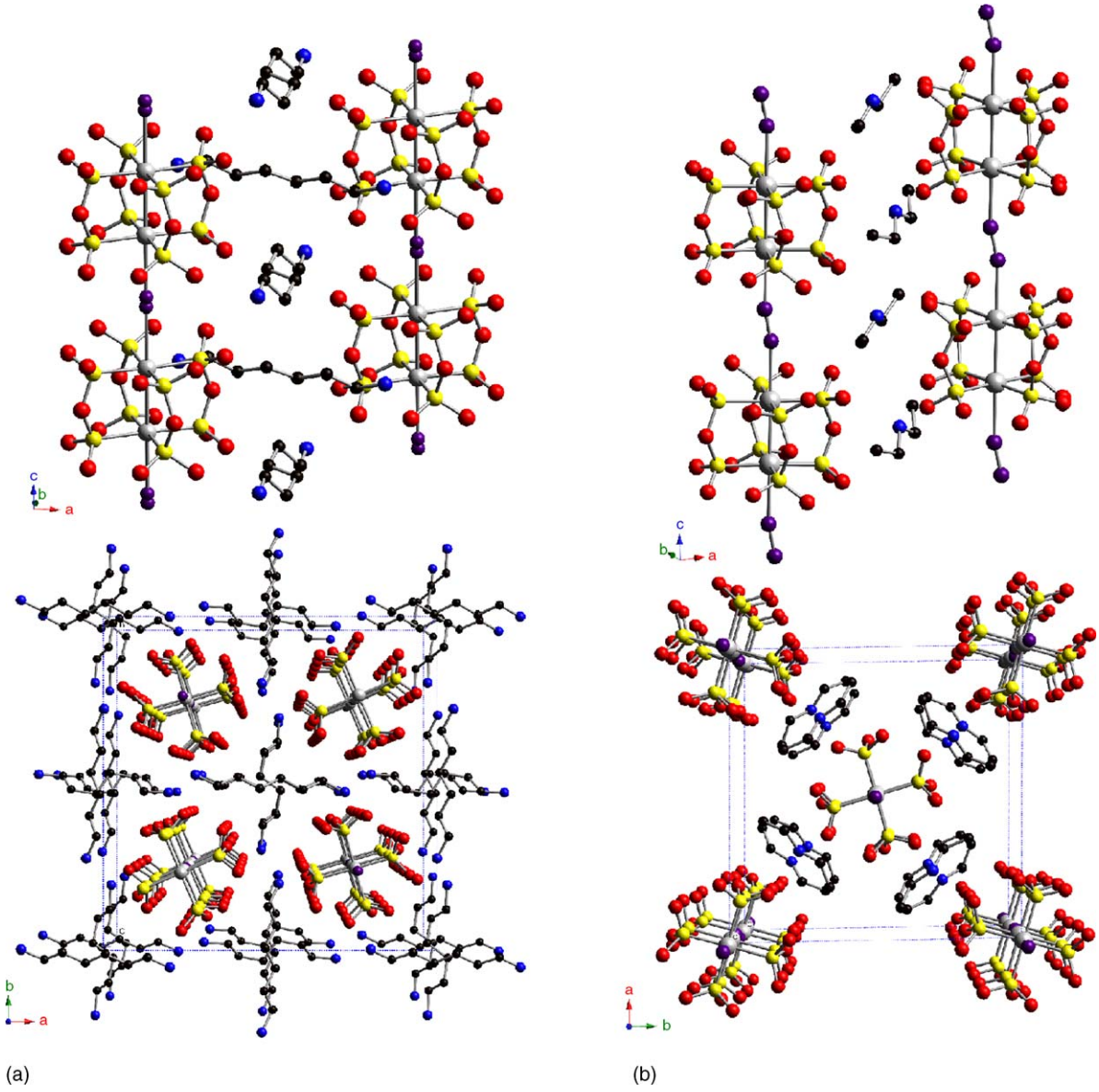

Fig. 1. Perspective views of crystal structures of (a) $[H_3N(C_6H_{12})NH_3]_2[Pt_2(pop)_4I]$ and (b) $[(C_2H_5)_2NH_2]_4[Pt_2(pop)_4I]$.

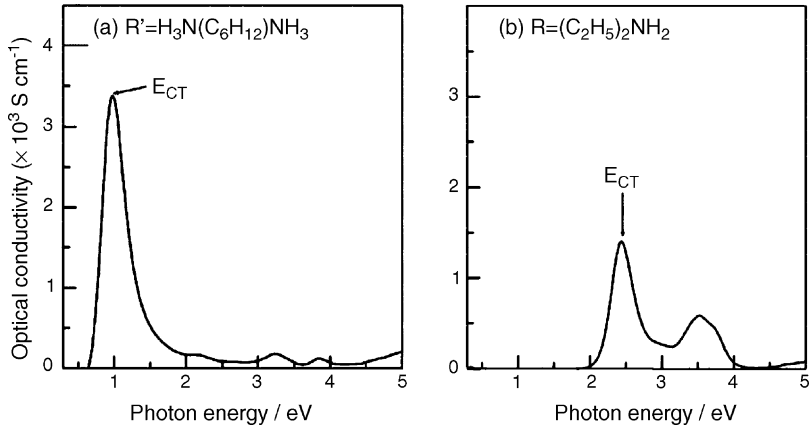

Fig. 2. Optical conductivity spectra of (a) $[H_3N(C_6H_{12})NH_3]_2[Pt_2(pop)_4I]$ and (b) $[(C_2H_5)_2NH_2]_4[Pt_2(pop)_4I]$.

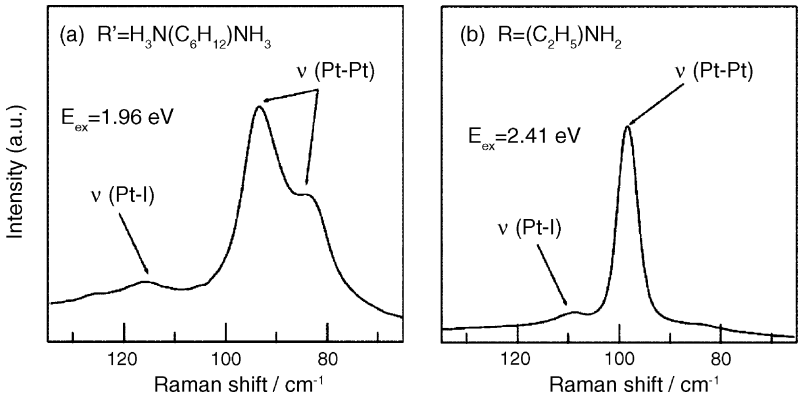

Fig. 3. Raman spectra of (a) $[H_3N(C_6H_{12})NH_3]_2[Pt_2(pop)_4I]$ and (b) $[(C_2H_5)_2NH_2]_4[Pt_2(pop)_4I]$.

origin. On the other hand, in the $[(C_2H_5)_2NH_2]_4[Pt_2(pop)_4I]$, the temperature dependence of χ_{spin} cannot be explained by the Curie component alone. There is a finite component independent of temperature, that is attributed to a contribution from the 1D spin chain. The temperature independent component can be explained by the Bonner-Fisher (BF) curve, applicable to the 1D Heisenberg antiferromagnetic $S = 1/2$ chain. The Bonner-Fisher (BF) curve gives an almost temperature independent χ_{spin} value when the exchange interaction J/k_B is much larger than 300 K. The result in Fig. 4 (lower figure) can be roughly reproduced by the summation of the BF curve with $J/k_B \sim 3000$ K and a Curie component with the concentration of 0.34% per Pt site. From these comparative studies, we conclude that the ground states of $[(C_2H_5)_2NH_2]_4[Pt_2(pop)_4I]$ and $[NH_3(C_6H_{12})NH_3]_2[Pt_2(pop)_4I]$ are the CP and CDW states, respectively.

The phase diagram shown in Fig. 5 was compiled based on the systematic optical, magnetic, and X-ray studies on Pt–Pt–I chains with a series of ammonium cations. This figure shows the optical gap energies E_{CT} as a function of Pt···Pt distances in the Pt–I–Pt geometries d(Pt–I–Pt). The ground state changes from the CP to CDW with decreasing d(Pt–I–Pt), and there is a clear boundary at around 6.1 Å. In both states, linear relationships between E_{CT} and d(Pt–I–Pt) are observed.

Here let us discuss the stability of the CP and CDW states as a function of d(Pt–I–Pt), taking account of the theoretical studies based on the one-band extended Peierls-Hubbard model [33,34]. When d(Pt–I–Pt) is large, the intra-dimer Coulomb interaction V_{MM} and the intra-dimer transfer energy t_{MM} are important parameters dominating the ground state in addition to the on-site Coulomb repulsion U_M on Pt and the site-diagonal-type electron-lattice interaction β. The inter-dimer interaction such as the transfer energy t_{MXM}, the Coulomb interaction V_{MXM}, and the second nearest neighbor Coulomb interaction V_2 can be neglected. A simple picture is given by consideration of the localized limit ($t_{MM} = 0$). In this case, the relative energy of the CP and CDW states is determined by V_{MM}. The summation of the Coulomb energy for two neighboring Pt-dimers in the CDW

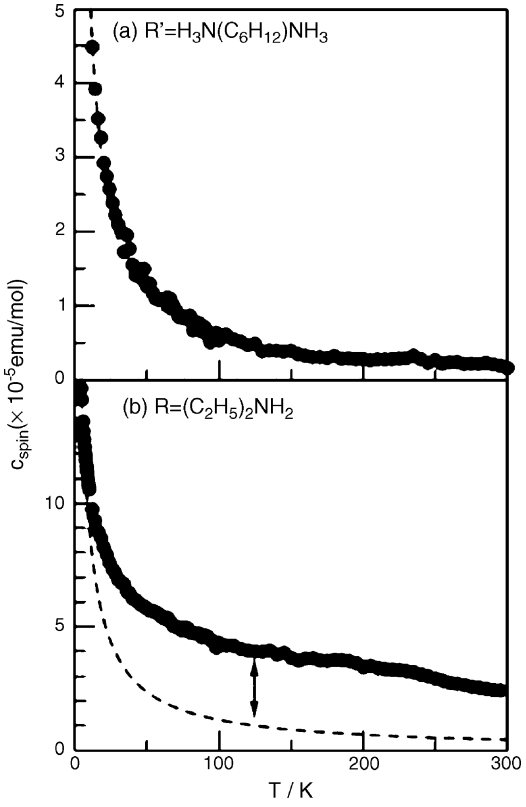

Fig. 4. Magnetic susceptibilities of (a) $[H_3N(C_6H_{12})NH_3]_2[Pt_2(pop)_4I]$ and (b) $[(C_2H_5)_2NH_2]_4[Pt_2(pop)_4I]$.

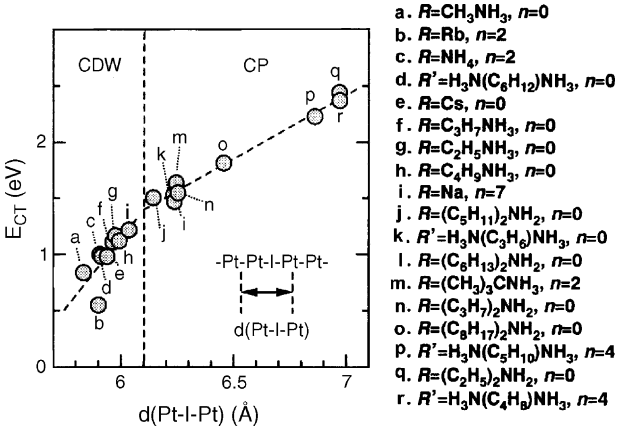

Fig. 5. Optical gap energy E_{CT} of a series of iodide-bridged binuclear Pt compounds as a function of Pt···Pt distance in the Pt–I–Pt geometry.

($5V_{MM}$) is larger than that in the CP ($4V_{MM}$). Therefore, V_{MM} stabilizes the CP state. Under the presence of t_{MM}, the bonding orbital in the Pt dimer is formed in the CP state, but not formed in the CDW state because of large U_M. As a result, t_{MM} also stabilizes the CP state. As d(Pt–I–Pt) decreases, V_{MXM}, V_2, t_{MXM}, and β will increase. The increase of V_2 makes the CP state rather unstable, while V_{MXM} does not affect the relative energy of the CP and CDW states. The effects of t_{MXM} and β are not so straightforward. The theoretical calculations have revealed that the increase of β and t_{MXM} also stabilizes the CDW state relatively to the CP state. Thus, the theoretical studies can explain well the experimental result that the ground state changes from the CP state to the CDW state with decrease of d(Pt–I–Pt).

In summary, we have synthesized iodide-bridged dinuclear Pt compounds with alkylammonium and alkyldiammonium counteractions. By modulating of the interdimer distance d(Pt–I–Pt) by the substitution of counteractions, the electronic state was switched between the CDW and CP states.

3. Phase transitions by pressure and photo-irradiation in MMX chain compounds

The control of the phase transitions and related macroscopic properties by photo-irradiation has recently attracted much attention. This phenomenon is called as a photo-induced phase transition (PIPT) and is important not only as a new phenomenon in the fields of chemistry and physics, but also as a useful mechanism applicable to future optical switching devices. A key strategy toward realizing PIPT is the exploration of one-dimensional materials, because the 1D electronic states essentially include strong instabilities inherent to the electron-lattice and/or electron–electron interactions and sometimes produce the characteristic phase transitions at low temperature or by the pressure. The PIPTs have been driven in a π-conjugated polymer (polydiacetylene) [35] and an organic charge transfer complex tetrathiafulvalene-*p*-chloranil (TTF-CA) [36] by irradiation of the light near the phase transition temperature. However, the PIPTs in 1D electronic systems are limited to these organic materials. No PIPTs have been found in 1D transition metal complexes and other 1D inorganic materials so far. Moreover, polydiacetylene and TTF-CA are always diamagnetic, and their magnetic properties do not change appreciably in their PIPTs. On the other hand, in the CDW and CP states in MMX chain compounds, their magnetic properties change from diamagnetic to antiferromagnetic states. If the oxidation states of the compounds are three-dimensionally ordered, multi-functional switching properties can be realized such as switching between para- and ferro-dielectrics, and switching between second-order ($\chi^{(2)}$) and third-order ($\chi^{(3)}$) optical non-linearity as a consequent of the change of the symmetry. According to such strategies, we have tried to realize the phase transition between the CP and CDW state in MMX chain compounds.

From the phase diagram in Fig. 5, it is expected that a phase transition can be driven by applying pressure to the materials in the CP states. Such a pressure-induced phase transition (PRIPT) from the CP to CDW state has indeed been observed for the materials, $[(C_2H_5)_2NH_2]_4[Pt_2(pop)_4I]$, $[(C_5H_{11})_2NH_2]_4[Pt_2(pop)_4I]$ and $[(C_3H_7)_2NH_2]_4[Pt_2(pop)_4I]$. Photographs of the pressure-induced phase transition in $[(C_2H_5)_2NH_2]_4[Pt_2(pop)_4I]$ are presented in Fig. 6(a). At ambient pressure, the color of this compound is green. When the pressure is increased to 0.6 GPa, a brown region appears and grows gradually. Fig. 6(b) shows the change of the Raman spectra accompanying this pressure-induced phase transition. The ν(Pt–Pt) clearly splits at above 0.6 GPa, indicating that the high-pressure brown phase is the CDW state. Fig. 7(a) shows the pressure dependence of E_{CT}, obtained from an analysis of the polarized reflectivity spectra. The phase transition is a first-order reversible with a large hysteresis loop (ca. 0.4 GPa).

Images of the crystal reveal that the sample size along the chain axis *c* is reduced by ca. 8% under 0.85 GPa pressure, from ambient pressure. If, assuming that the Pt–Pt distance d(Pt–Pt) of the Pt–Pt unit does not change under pressure, d(Pt–I–Pt) at 0.85 GPa is estimated to be 6.2 Å. This assumption is reasonable because d(Pt–Pt) is almost constant in the various MMX chain compounds. The values obtained, d(Pt–I–Pt) = 6.2 Å and E_{CT} = 1.6 eV at 0.85 GPa, are very close to those in the CDW state (see Fig. 5). That is, the pressure-induced phase transition from the CP to CDW state is driven by a decrease in d(Pt–I–Pt).

At points *a* and *b* in Fig. 7a, the compound is in a metastable state. The photo-induced phase transition (PIPT) from the metastable state to the ground state at points *a* and *b* was investigated. Fig. 7(b) shows the images of the sample at a point before and after photo-irradiation with 2.41 eV light for 8 ms. As can be seen, the crystal exhibits a permanent color change from brown to green in the irradiation region. The Raman signal in the irradiated region is almost identical to that of the low-pressure phase, that is the CDW state. In order to clarify whether this PIPT is induced by an optical process or laser heating, the dependence of the PIPT efficiency on the excitation photon density *N* was investigated for two excitation energies E_{ex} of 1.96 and 2.41 eV. *N* was calculated considering the absorption coefficient and the reflection loss of the excitation light, and the converted fractions were estimated from the photo-induced changes in the integrated intensity of the Pt–Pt stretching Raman bands. The PIPT efficiency exhibits at *a* a clear threshold N_{th} (photon density per 8 ms pulse), the values of which are strongly dependent on E_{ex} ($N_{th} \sim 1.4 \times 10^{25}$ cm^{-3} at E_{ex} = 1.96 eV and $\sim 3 \times 10^{24}$ cm^{-3} at 2.41 eV). This characteristic excitation energy dependence of N_{th} demonstrates that the observed PIPT is driven not by laser heating but by an optical process. At *b*, the PIPT could not be driven by the irradiation of 1.96 or 2.41 eV light, even if the intensity and duration of the light were changed. However, irradiation with 2.71 eV light for 30 s did result in a PIPT, as shown in Fig. 7(b). As this process appears to be strongly dependent on the excitation energy, the PIPT from CP to CDW state is also attributable to an optical process, although the efficiency of the PIPT from the CP to CDW state is much lower than that from the CDW to CP state.

A previous theoretical study suggested that the lowest transition in the CDW state is an inter-dimer CT excitation from $[\cdots Pt^{2+}–Pt^{2+}\cdots I–Pt^{3+}–Pt^{3+}–I\cdots]$ to $[–I\cdots Pt^{2+}–Pt^{3+}–I\cdots Pt^{2+}–Pt^{3+}–]$. Therefore, an optical excitation in CDW state will produce a local CP state. This is the reason

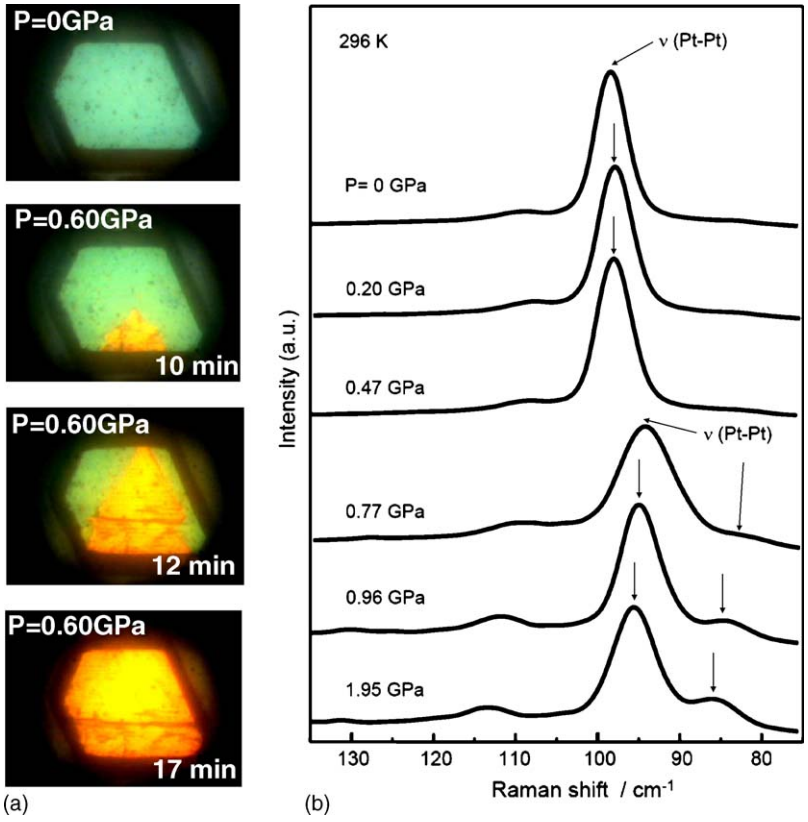

Fig. 6. (a) Microscope images and (b) Raman spectra of $[(C_2H_5)_2NH_2]_4[Pt_2(pop)_4I]$ under the external pressure.

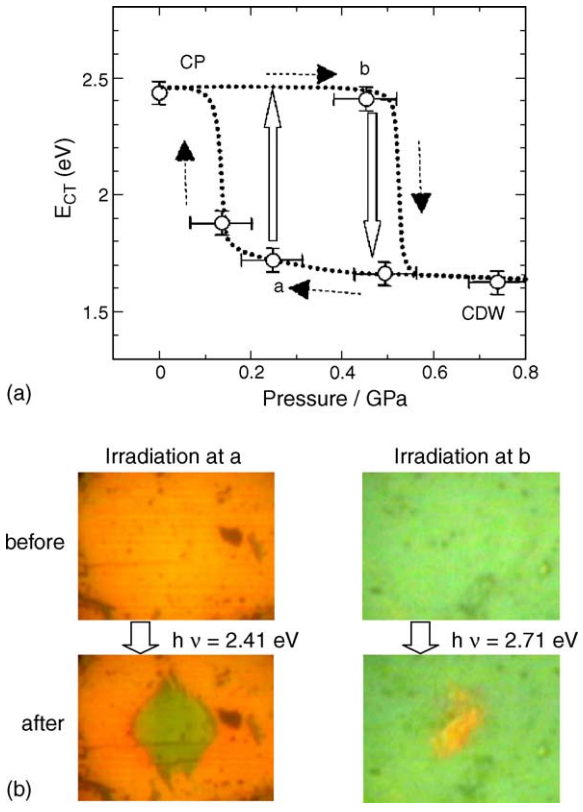

Fig. 7. (a) Pressure dependence of E_{CT}. (b) Microscope images at the points a and b before and after photoirradiation.

why the CDW state to CP state transition is readily induced by the photo-irradiation. In the CP state, on the other hand, intra-dimer CT transition from $[–I\cdots Pt^{2+}–Pt^{3+}–I\cdots Pt^{2+}–Pt^{3+}–]$ to $[\cdots I–Pt^{3+}–Pt^{2+}\cdots I\cdots Pt^{2+}–Pt^{3+}–I\cdots]$ is the dominant optical excitation corresponding to the gap transition. In this process, the CDW state is never produced, even as a local excited state. As a result, it is difficult to achieve the CP to CDW phase transition by photo-irradiation with the energy of 2.41 eV near equal to E_{CT}. As observed in the experiments, the 2.71 eV excitation drives the PIPT from the CP to CDW state, although the transition efficiency is very low. Such higher-energy excitation will induce the inter-dimer CT transition from $[–I\cdots Pt^{2+}–Pt^{3+}–I\cdots Pt^{2+}–Pt^{3+}–]$ to $[\cdots Pt^{2+}–Pt^{2+}\cdots I–Pt^{3+}–Pt^{3+}–I\cdots]$, which may be relevant to the PIPT to CDW state.

In summary, the PRIPT of $[(C_2H_5)_2NH_2]_4[Pt_2(pop)_4I]$ from the CP state to the CDW state was identified, exhibiting a large hysteresis loop, and the PIPT between the CDW and CP states was found to be drivable within this loop. This transition behavior is an exceptional example of the PIPT, demonstrating that it is possible to achieve fundamental changes in optical and magnetic properties through photo-irradiation alone.

4. Vapochromic behavior accompanied by phase change between CP state and CDW state in MMX chain compounds

Some one-dimensional materials have been shown to show striking and reversible changes in color and/or luminescence

upon exposure of volatile organic compounds and water vapor. This spectroscopic change in the presence of vapor is called vapochromism, which is a promising phenomenon for chemical-vapor-sensing devices. Mann and co-workers have reported vapochromic behavior in 1D Pt(II) compounds, $[Pt(CNR)_4][Pt(CN)_4]$ (R = *p*-CN–C_6H_4–C_nH_{2n+1}; $n = 1, 2, 6, 10, 12, 14$) [37]. Kato et al. have also reported the behavior in 1D Pt(II) complexes $[Pt(CN)_2(bpy)]$ (bpy = 2,2′-bipyridine), and syn-$[Pt_2(bpy)_2(pyt)_2][PF_6]_2$ (pyt = pyridine-2-thiolate ion)[38]. The vapochromic behavior of these compounds is driven by the change of the Pt···Pt distance which is connected by a weak metallophilic interaction, which is not related to instabilities of one-dimensional electronic structures such as Peierls and spin-Peierls instabilities.

We have found a new type of vapochromism accompanied with the phase change between the CDW and CP states, which is characteristic of one-dimensional electronic systems in MMX compounds. These compounds are $[NH_3(C_4H_8)NH_3]_2[Pt_2(pop)_4I]\cdot 4H_2O$ and $[NH_3(C_5H_{10})NH_3]_2[Pt_2(pop)_4I]\cdot 4H_2O$, which have four water molecules at room temperature.

Fig. 8 shows a perspective view of the crystal structure of $[NH_3(C_4H_8)NH_3]_2[Pt_2(pop)_4I]\cdot 4H_2O$ at 296 K. Two Pt ions are linked by four pop ligands to form a lantern type $[Pt_2(pop)_4]$ unit. The neighboring $[Pt_2(pop)_4]$ units are bridged by iodide ions, thus forming a Pt–Pt–I linear chain along *c*-axis. The bridging iodide ions are disordered with half occupancies from the midpoints between the neighboring Pt–Pt units, because displacement of iodide ions is not three-dimensionally ordered. Therefore, it is difficult to determine from X-ray structural analyses whether the ground state of this compound is the CDW or CP state. The Pt–Pt distance is 2.847 Å, which is between that in $K_4[Pt^{2+}{}_2(pop)_4]\cdot 2H_2O$ (2.925 Å) and that in $K_4[Pt^{3+}{}_2(pop)_4I_2]$ (2.754 Å), and Pt–I distance is 2.722 Å. The counteractions $[NH_3(C_4H_8)NH_3]^{2+}$ are located in the spaces among the four chains and form hydrogen-bonds to the oxygen atoms of the pop ligands. Four H_2O molecules are also located in the spaces.

Raman spectra were measured to obtain the information about the electronic structure of this compound. Fig. 9 shows the polarized Raman spectra of this compound in the usual laboratory humidity at 296 and 340 K. The strong signals at 80–100 cm^{-1} are attributed to the Pt–Pt stretching mode ν(Pt–Pt) of the Pt–Pt units. The overtone progressions of ν(Pt–Pt) up to fourth order are observed in both spectra. At 296 K, a singlet ν(Pt–Pt) mode is observed at 98 cm^{-1}, which indicates the formation of only one kind of Pt–Pt unit. A relatively weak band is also observed at around 115 cm^{-1}. This band can be assigned to the Pt–I stretching mode. This fact is consistent with the crystal structure of this compound discussed above. Therefore, the electronic state of this compound at 296 K can be considered as the CP state. On the other hand, the ν(Pt–Pt) band clearly splits into two components when the temperature is increased from 296 to 340 K, indicating that there are two kinds of Pt–Pt units, namely Pt^{2+}–Pt^{2+} (86 cm^{-1}) and Pt^{3+}–Pt^{3+} (94 cm^{-1}), while the Pt–I stretching mode seems still to be activated. Therefore, the electronic state at 340 K is reasonably attributable to the CDW state.

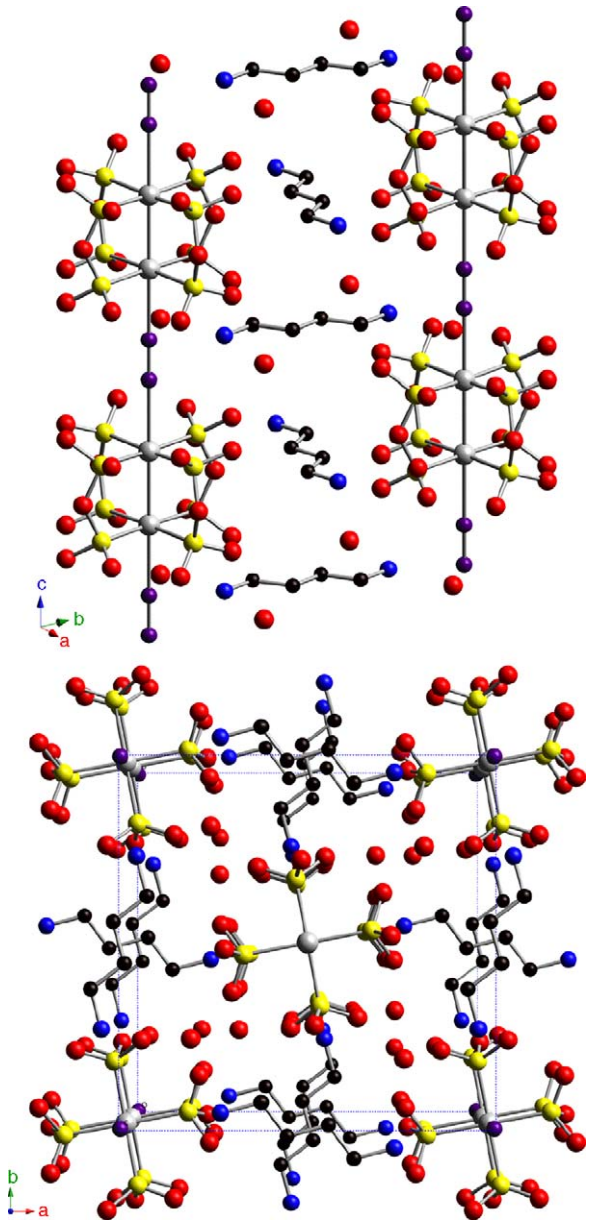

Fig. 8. Perspective view of crystal structure of $[N_3N(C_4H_8)NH_3]_4[Pt_2(pop)_4I]$. Gray: Pt, purple: I, yellow: P, red: O, black: C and blue: N.

The temperature dependence of the magnitude of splitting in the Pt–Pt stretching Raman band $\Delta\nu$(Pt–Pt) is shown in Fig. 9b. When heated from room temperature, $\Delta\nu$(Pt–Pt) remains at zero within the temperature range from 296 to 330 K but abruptly increases to about 10 cm^{-1} at 333 K. In the cooling run, $\Delta\nu$(Pt–Pt) does not change even at 333 K, but returns to zero at 300 K. This result indicates that the CDW state can return to the original CP state by cooling the crystal to room temperature. We confirmed this reversibility by repeating the heating and cooling processes several times. The reversibility largely depends on the humidity. In fact, the CDW state does not recover to the CP state on lowering the temperature in a fully dry atmosphere. However, we can obtain reversibility by exposing the crystal to water vapor. Thus, the reversibility is not a simple function of temperature.

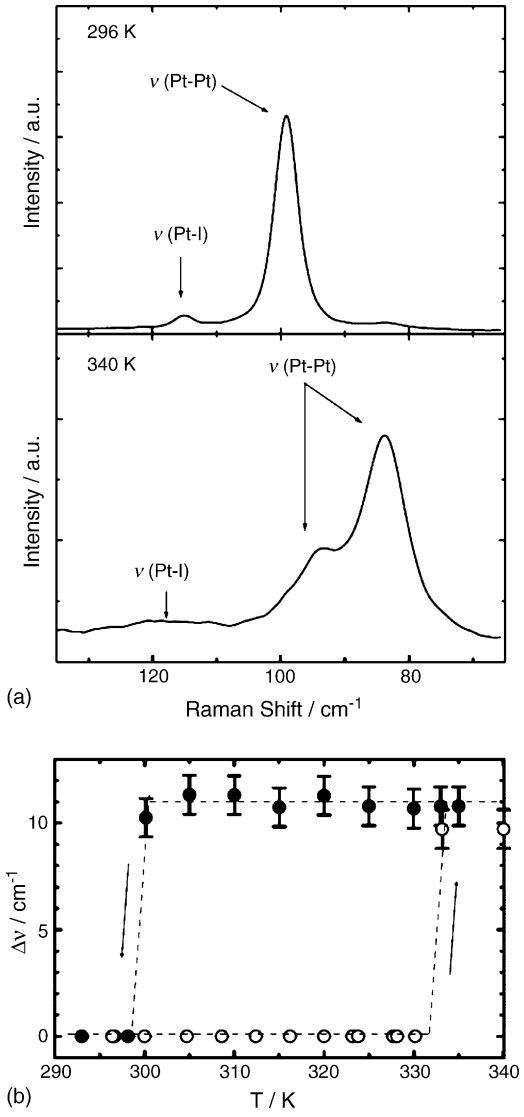

Fig. 9. (a) Raman spectra of $[N_3N(C_4H_8)NH_3]_4[Pt_2(pop)_4I]$ at 296 and 340 K. (b) Temperature dependence of the magnitude of spectrum splitting in the Pt–Pt stretching Raman band ν(Pt–Pt). Broken line shows guide to eye.

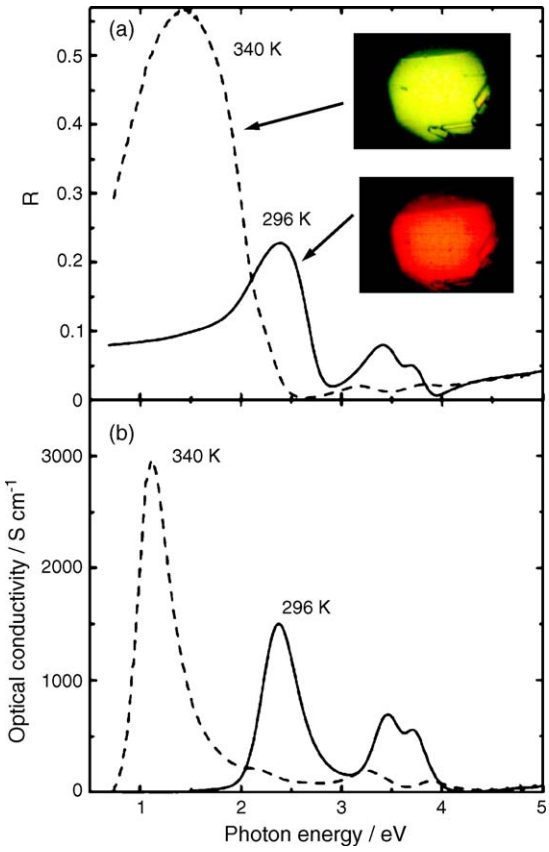

Fig. 10. (a) Polarized reflectivity and (b) optical conductivity spectra in $[N_3N(C_4H_8)NH_3]_4[Pt_2(pop)_4I]$ at 296 and 340 K. The insets in (a) show the corresponding microscope images for the single-crystal taken in reflection mode.

The most striking feature of this compound is that the CP-to-CDW phase change is accompanied by a marked color change of the crystal. The polarized reflectivity spectra and corresponding microscope images of the sample are presented in Fig. 10a. This compound is yellow–green at 296 K as a result of the peak at 2.37 eV, while on increasing the temperature up to about 340 K, the color changes to red–brown. This color is primarily a result of the strong reflection band from the near-infrared to visible region. Such clear chromism is also confirmed by the optical conductivity (σ) spectra (Fig. 10). The peak energy of the lowest CT band drastically shifts from 2.37 eV (520 nm) to 1.12 eV (1110 nm). This spectral change is anomalously larger than that of the previously reported vapochromic materials. From the previous theoretical study on the optical excitation in the MMX chain compounds, the lowest CT band observed at 2.37 eV in the CP phase can be assigned to intra-dimer CT excitation from $[–I\cdots Pt^{2+}–Pt^{3+}–I\cdots Pt^{2+}–Pt^{3+}–I\cdots]$ to $[–I–Pt^{3+}–Pt^{2+}\cdots I\cdots Pt^{2+}–Pt^{3+}–I–]$, while the CT band at 1.12 eV in the CDW phase is attributable to the inter-dimer CT band from $[–I\cdots Pt^{2+}–Pt^{2+}\cdots I–Pt^{3+}–Pt^{3+}–I–]$ to $[–I\cdots Pt^{2+}–Pt^{3+}–I\cdots Pt^{2+}–Pt^{3+}–I–]$. The CP-to-CDW phase change and the resultant change of the origin for the optical gap are responsible for the observed chromism. The gap energy $E_{CT} = 1.12$ eV at 340 K is nearly equal to that of other compounds in the CDW phase. The d(Pt–I–Pt) value is relatively small in the CDW compounds compared to that in the CP compounds. Therefore, it is reasonable to consider that the observed CP-to-CDW change is driven by the decrease in the value of d(Pt–I–Pt).

Thermogravimetric analysis (TGA) was performed in a dry nitrogen atmosphere to obtain an insight into the mechanism of the CP-to-CDW phase change (Fig. 11). This compound shows a gradual weight loss when the temperature is increased from the room temperature, and has lost 5.450% of its weight at 395 K. This value is in good agreement with that calculated (5.365%) for the loss of four H_2O molecules per formula unit. Powder X-ray diffraction measurements were also performed to investigate the vapochromic structural changes. The diffraction pattern of this compound heated at 353 K in vacuum shows that the crystal has converted into some new, and as yet unidentified, crystal structure. With decreasing the temperature, X-ray powder pat-

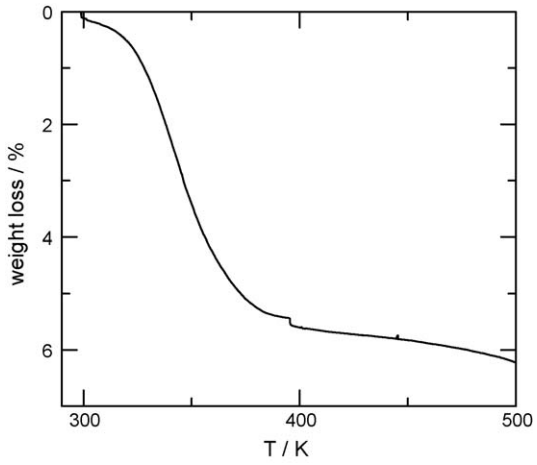

Fig. 11. TGA trace of $[N_3N(C_4H_8)NH_3]_4[Pt_2(pop)_4I]$ under a dry nitrogen purge at 5 K min^{-1}.

tern at 296 K was almost recovered and consistent with that before heating.

The species $[NH_3(C_5H_{10})NH_3]_2[Pt_2(pop)_4I]\cdot 4H_2O$ also shows vapochromic behavior accompanied by a phase change between CP state and CDW state. At 297 K, the $[NH_3(C_5H_{10})NH_3]_2[Pt_2(pop)_4I]\cdot 4H_2O$, having four water molecules, shows the singlet $\nu(Pt^{2+}–Pt^{3+})$ Raman mode at 98.3 cm^{-1} and intra-dimer charge transfer band from Pt^{2+} to Pt^{3+} around 2.24 eV. This compound is in the CP state at this temperature. With increasing temperature, Raman stretching mode splits into 86.4 and 93.9 cm^{-1} (340 K) and charge transfer band shifts to 1.14 eV (340 K) together with the loss of the water molecules. This indicates that the electronic state of this compound changed from the CP to CDW with increasing temperature (losing water molecules). Such vapochromic behavior accompanied by a phase change has occurred repeatedly and is more easily compared with those of $[NH_3(C_4H_8)NH_3]_2[Pt_2(pop)_4I]\cdot 4H_2O$ due to the larger inter-chain spaces of $[NH_3(C_5H_{10})NH_3]_2[Pt_2(pop)_4I]\cdot 4H_2O$ with the larger counter cations (the space for $[NH_3(C_4H_8)NH_3]_2[Pt_2(pop)_4I]\cdot 4H_2O$ is 3.3×1.6 $Å^2$ and that for $[NH_3(C_5H_{10})NH_3]_2[Pt_2(pop)_4I]\cdot 4H_2O$ is 6.8×1.7 $Å^2$).

5. Metal-insulator transition relating to charge-ordering state of $Pt_2(RCS_2)_4I$ (R: alkyl-chain group)

In the preceding sections, we described the phase control of the pop system by changing the counter cations, and showed the various phase transitions driven by the external stimuli such as pressure, photoirradiation and temperature. In this section, we describe the various phase transitions in the $Pt_2(RCS_2)_4I$ (R = alkyl chains), which are the consequence of the competition between electron–electron and electron–lattice interactions characteristic of the 1D system.

The structures of the first metallic halogen-bridged 1D chain complex $Pt_2(dta)_4I$ (dta: dithioacetato, $n = 1$; n is the number of C atoms in RCS_2 ligand), and its analogue $Pt_2(dtp)_4I$ (dtp: dithiopropionato, $n = 2$) are shown in Fig. 12. The 1D chain structure constructed by Pt dimer with bridging iodide is similar to that of the pop complex mentioned above except for the absence of a counter cation. The inter-chain distance can be modulated by the length of alkyl-chain in the dta ligand, and the physical properties of these dta-type complexes are very sensitive to the length of alkyl-chain. The nearest neighbor inter-chain distances of $Pt_2(dta)_4I$ and $Pt_2(dtp)_4I$ are 6.82 and 8.32 Å, respectively. The weak S···S contact between 1D chains exists in $Pt_2(dta)_4I$, but it is lost by the longer alkyl-chain in $Pt_2(dtp)_4I$. The Pt–Pt distance (2.68 Å) is significantly shorter, by about 0.2 Å, than in the pop-type complex (2.85 Å) which is an important feature of dta-type complexes.

Fig. 13 shows the temperature dependences of electrical resistivity along 1D chain axis of $Pt_2(dta)_4I$ and $Pt_2(dtp)_4I$. As is clearly seen, both complexes are highly conductive (ca. 10 S cm^{-1}) and exhibit metallic conductivity, but the temperature dependences of these complexes are significantly different. The electronic state in the metallic region of both complexes can be assigned basically to the AV state. Thermoelectric power property indicates the gapless structure at the Fermi energy, which also suggests the AV state of the compound. It is surprising that the metal-insulator transition temperature T_{MI} in $Pt_2(dtp)_4I$ ($T_{MI} = 205$ K) is much lower than that in $Pt_2(dta)_4I$ ($T_{MI} = 300$ K), by about 100 K, because the existence of S···S contact between 1D chains in $Pt_2(dta)_4I$ would suppress the

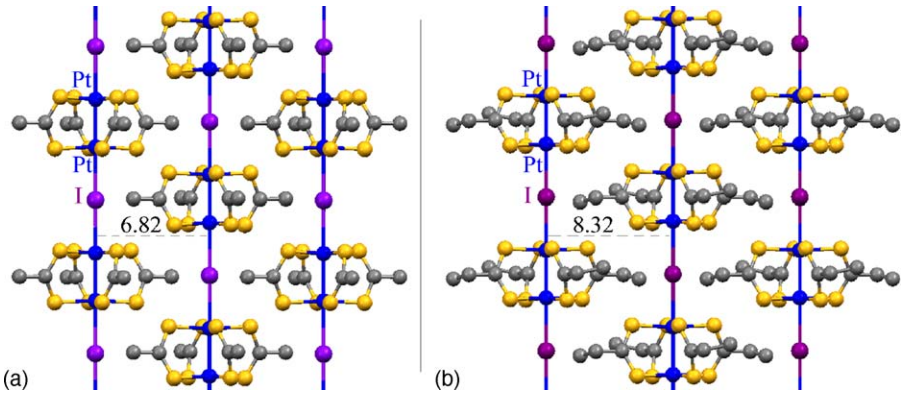

Fig. 12. 1D chain structures of (a) $Pt_2(dta)_4I$ and (b) $Pt_2(dtp)_4I$. The values displayed in figures indicate the nearest neighboring inter-chain distance.

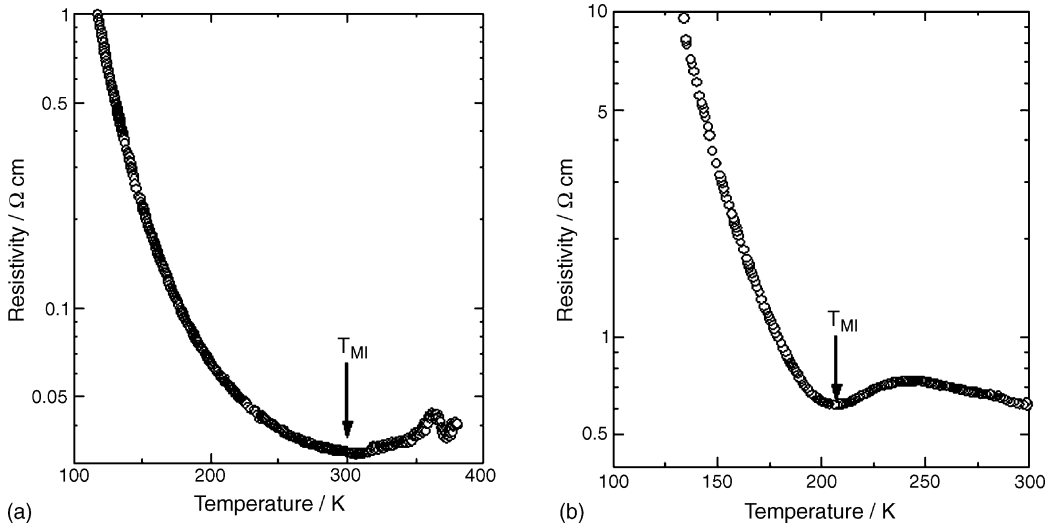

Fig. 13. Temperature dependences of electrical resistivity of (a) $Pt_2(dta)_4I$ and (b) $Pt_2(dtp)_4I$.

Peierls instability which is a well known origin of metal-insulator transition in 1D electronic system. Moreover, the electrical resistivity of $Pt_2(dtp)_4I$ above $T_{MI} = 205$ K is not explained as a normal metallic state. Although the thermoelectric power for $Pt_2(dtp)_4I$ indicates the gapless structure at the Fermi level above T_{MI}, metallic behavior is observed only between T_{MI} and 235 K. Above 235 K, the resistivity decreases with increasing temperature, indicating semiconducting behavior. According to the X-ray diffraction study by Mitsumi et al. [21], X-ray diffuse scatterings characterized by the wave-vector $b^*/2$ (b^* corresponds to 1D chain axis) are observed, and the diffuse scattering shape changes from a line lying on the a^*-axis to planes at about 235 K, suggesting that the dimensionality of two-fold periodic ordering on 1D chain significantly contributes to the electronic conductivity of $Pt_2(dtp)_4I$. Our recent study on diffuse scattering has revealed that the two-fold periodic ordering on 1D chain corresponds to the CDW state [39].

The magnetic susceptibility also depends on the length of alkyl-chain in the dta ligand. The temperature dependences of magnetic susceptibility of $Pt_2(dta)_4I$ and $Pt_2(dtp)_4I$ are shown in Fig. 14. In the metallic region of $Pt_2(dta)_4I$ above 300 K, the magnetic susceptibility decreases with temperature. This magnetic susceptibility decrease can be explained by an antiferromagnetic interaction between the spins on adjacent $Pt^{2.5+}$-dimers through the p_z orbital of the bridging iodide due to a superexchange interaction. On the other hand, the susceptibility of $Pt_2(dtp)_4I$ above T_{MI} decreases slightly with increasing temperature. The susceptibility is one order of magnitude lower than that of $Pt_2(dta)_4I$, which would correspond to the existence of two-fold structure of diamagnetic CDW state. In the semiconducting region below T_{MI} in both complexes, the susceptibility increases gradually with decreasing temperature, indicating that the metal-insulator transition originates not from the Peierls transition but from the Mott-Hubbard transition. If the metal-insulator transition of these complexes relates to the Peierls instability, the spin susceptibility should be lost below T_{MI} due to the freezing of both charge and spin degrees of freedom. Conversely, in the case of Mott-Hubbard transition, the charge degree

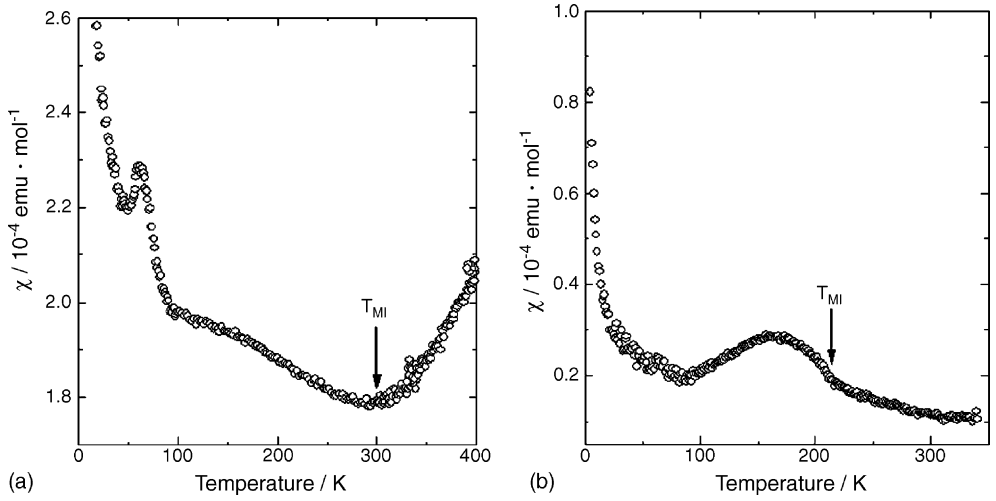

Fig. 14. Temperature dependence of magnetic susceptibility of (a) $Pt_2(dta)_4I$ and (b) $Pt_2(dtp)_4I$.

of freedom is lost, but the spin degree of freedom is maintained. Considering the maintenance of the spin degree of freedom, the electronic state on MMX-chain changes from the metallic AV state to semiconducting CP state at T_{MI}. Since some anomalies are observed in the magnetic susceptibility of $Pt_2(dta)_4I$ below 90 K, there seem to be several transitions which relate to spin degree of freedom. The magnetic susceptibility of $Pt_2(dtp)_4I$ also decreases gradually below 160 K, suggesting some electronic structural changes at low temperature range.

To clarify the electronic state at low temperature range of these complexes, ^{129}I Mössbauer spectroscopic measurements were performed. ^{129}I Mössbauer spectroscopy is a powerful technique to investigate the electronic state of the iodide complex at low temperature. Since the ^{129}I nuclear spin states of ground and excited states are 7/2 and 5/2, respectively, the quadrupole-split spectra consist of a minimum of eight lines. The observed Mössbauer data, isomer shift (IS), nuclear quadrupole coupling constant (QCC), the number of p-hole (h_p), the p-electron imbalance (U_p), and the relative intensity (area) for $Pt_2(dta)_4I$, $Pt_2(dta)_4I$ and their Pt^{3+}-dimer precursors $Pt_2(dta)_4I_2$ and $Pt_2(dtp)_4I_2$ are given in Table 1.

Very similar ^{129}I Mössbauer parameters of $Pt_2(dta)_4I_2$ and $Pt_2(dtp)_4I_2$ suggest that the difference of alkyl-chain length in dta ligand scarcely affects the electronic state of Pt^{3+}-dimer. Nevertheless the physical properties of MMX-chain complexes with dta derivatives depend on the alkyl-chain length, indicating the significance of the inter-chain interaction. Fig. 15 shows the ^{129}I Mössbauer spectra of $Pt_2(dta)_4I$ at 16 K and $Pt_2(dtp)_4I$ at 11 K. The best fit for each spectrum was obtained by two octuplets, signifying that there are two chemically independent iodide sites in these MMX-chain complexes at low temperature. The spectra of both complexes at 80 K also consist of two octuplets. Therefore, these results strongly suggest that the electronic state corresponds to the ACP state which is analogous to the diamagnetic spin-Peierls state and has two chemically independent iodide sites as following: $\cdots Pt^{2+}–Pt^{3+}–I_A–Pt^{3+}–Pt^{2+}\cdots I_B\cdots$. Regarding the ACP state as the low temperature state, the magnetic susceptibility decreasing below 90 K in $Pt_2(dta)_4I$ and below 160 K in $Pt_2(dtp)_4I$ can be explained by the development of the diamagnetic ACP state.

Table 1
^{129}I Mössbauer data for $Pt_2(dta)_4I$, $Pt_2(dtp)_4I$ and their Pt^{3+}-dimer precursors

Iodide site	T (K)	IS[a] (mm s^{-1})	QCC (MHz)	h_p	U_p	Area
Pt^{3+}-dimer precursors						
$Pt_2(dta)_4I_2$	16	3.66	−1172	0.47	0.51	
$Pt_2(dtp)_4I_2$	16	3.71	−1177	0.51	0.51	
$Pt_2(dta)_4I$						
A	16	3.77	−1180	0.55	0.51	1.27
B		4.05	−1380	0.73	0.60	1.00
A	80	3.71	−1184	0.51	0.52	1.07
B		3.99	−1390	0.69	0.61	1.00
$Pt_2(dtp)_4I$						
A	11	3.84	−1213	0.59	0.53	0.85
B		3.99	−1432	0.69	0.62	1.00
A	80	3.80	−1238	0.56	0.54	0.79
B		3.95	−1413	0.67	0.62	1.00

[a] Referenced to Mg_3TeO_6.

^{129}I Mössbauer parameters enable one to discuss quantitatively the electronic state of the bridging iodide. Assuming the ACP state, the intensity ratio of the two components should be primarily 1.0, the I_A/I_B compositional ratio in stoichiometric $Pt_2(dta)_4I$ and $Pt_2(dtp)_4I$. The deviation of observed intensity ratio I_A/I_B (area) from 1.0 is considered to originate from the difference of recoil-free fraction between I_A and I_B sites. In $Pt_2(dta)_4I$, the intensity of the I_A site having a small QCC absolute value is larger than that of I_B, suggesting that the environment of I_A anion is more rigid than that of I_B. Both IS and QCC values enable one to estimate the electron population (p-hole number h_p and p-electron imbalance U_p, respectively) of the bridging iodides. The estimated charges on I_A and I_B are −0.4 and −0.3, respectively. The I_A anion has the almost the same electron density with that of Pt^{3+}-dimer precursors. On

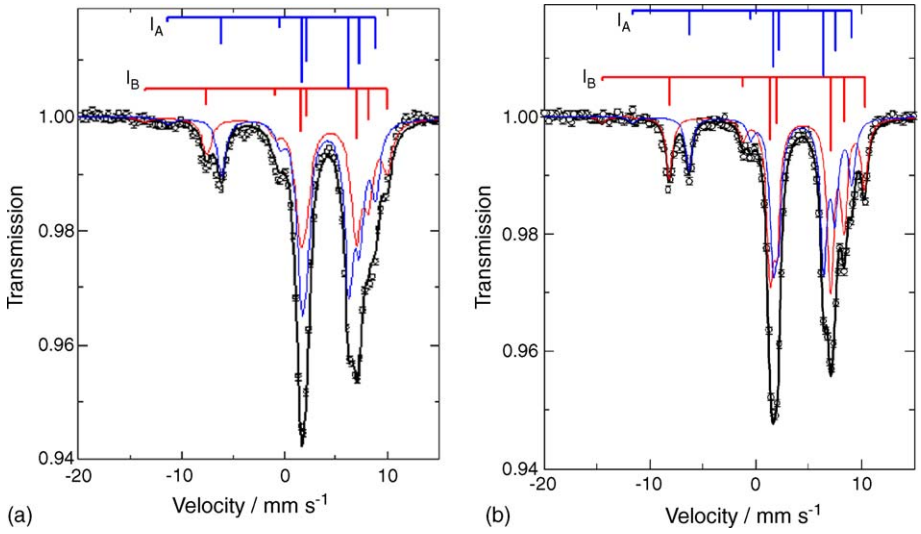

Fig. 15. ^{129}I Mössbauer spectra of (a) $Pt_2(dta)_4I$ at 16 K and (b) $Pt_2(dtp)_4I$ at 11 K.

the other hand, the I_B anion becomes more neutral owing to electron donation to the adjacent Pt-dimer. Considering these results, the Coulomb interaction plays a key role in the charge-ordering of this 1D electron system. The Mössbauer parameters of $Pt_2(dtp)_4I$ and their temperature dependence are almost the same as those of $Pt_2(dta)_4I$ except for the relative intensity. This may be derived from the difference of the dimensionality of the ACP state; $Pt_2(dtp)_4I$ has a three-dimensionally ordered ACP state at 48 K, but the ACP state of $Pt_2(dta)_4I$ is ordered only one- or two-dimensionally.

In summary, we have found that two metallic MMX-chain complexes, $Pt_2(dta)_4I$ and $Pt_2(dtp)_4I$, exhibit metal-insulator transitions related to the Mott-Hubbard transition. The physical properties of dta-type complexes strongly depend on the alkyl-chain length of the dta ligand, which controls the inter-chain distance. Considering the temperature dependence of the electrical resistivity and magnetic susceptibility, the metallic and semiconducting states are considered to be the AV and CP states, respectively. At low temperatures, the ACP state, which is analogous to the spin-Peierls state, develops gradually and is finally ordered three-dimensionally in $Pt_2(dtp)_4I$. The other dta-type complexes with longer alkyl-chain have been reported recently, and exhibit high electrical conductivity and the ACP state as ground state. The metallic behavior and temperature sensitive electronic state observed in dta-type complexes would be related to the ACP state, because this state has not been obtained in the pop-type complexes.

6. Conclusion

In this review, we described the phase transitions driven by the external stimuli such as pressure, photoirradiation, humidity and temperature. These phase transitions are interesting from the viewpoint not only of pure science but also of applied science because such phase transitions can be applied to switching devices. For example, by considering the symmetry of the crystal structure, the crystal of the CDW state has an inversion center at the center of the Pt–Pt unit, while the crystal of the CP state has no inversion center. By using such a difference of symmetry, dielectric and non-linear optical properties can be switched. Our final goal is to realize "multi-functional devices" in the present compound, but many challenges remain before we reach this goal.

References

[1] B.K. Chakraverty, J. Phys. Lett. 40 (1979) L99.
[2] H.J. Keller, in: J.S. Miller (Ed.), Extended Linear Chain Compounds, Vol. 1, Plenum, New York, 1982, p. 357.
[3] P. Day, in: H.J. Keller (Ed.), Low-Dimensional Cooperative Phenomena, Plenum, New York, 1974, p. 191.
[4] R.J.H. Clark, in: D.E. Brown (Ed.), Mixed Valence Compounds, Reidel, Dordrecht, 1982, p. 271.
[5] H. Okamoto, M. Yamashita, Bull. Chem. Soc. Jpn., Accounts 71 (1998) 2023.
[6] M. Yamashita, T. Manabe, T. Kawashima, H. Okamoto, H. Kitagawa, Coord. Chem. Rev. 190–192 (1999) 309.
[7] H. Okamoto, K. Toriumi, T. Mitani, M. Yamashita, Phys. Rev. B42 (1990) 10381.
[8] S. Takaishi, Y. Tobu, H. Kitagawa, A. Goto, T. Shimizu, T. Okubo, T. Mitani, R. Ikeda, J. Am. Chem. Soc. 126 (2004) 1614.
[9] H. Kishida, H. Matsuzaki, H. Okamoto, T. Manabe, M. Yamashita, Y. Taguchi, Y. Tokura, Nature 405 (2000) 929.
[10] C. Bellitto, A. Flamini, L. Gastaldi, L. Scaramuzza, Inorg. Chem. 22 (1983) 444.
[11] C. Bellitto, G. Dessy, V. Fares, Inorg. Chem. 24 (1985) 2815.
[12] M. Yamashita, Y. Wada, K. Toriumi, T. Mitani, Mol. Cryst. Liq. Cryst. 216 (1992) 207.
[13] C.-M. Che, F.H. Herbstein, W.P. Schaefer, R.E. Marsh, H.B. Gray, J. Am. Chem. Soc. 105 (1983) 4604.
[14] M. Kurmoo, R.J.H. Clark, Inorg. Chem. 24 (1885) 4420.
[15] R.J.H. Clark, M. Kurmoo, H.M. Dawes, M.B. Hursthouse, Inorg. Chem. 25 (1986) 409.
[16] L.G. Butler, M.H. Zietlow, C.-M. Che, W.P. Schaefer, S. Sridhar, P.J. Grunthaner, B.I. Swanson, R.J.H. Clark, J. Am. Chem. Soc. 110 (1988) 1155.
[17] M. Yamashita, K. Toriumi, Inorg. Chim. Acta 178 (1990) 143.
[18] M. Yamashita, S. Miya, T. Kawashima, T. Manabe, T. Sonoyama, H. Kitagawa, T. Mitani, H. Okamoto, R. Ikeda, J. Am. Chem. Soc. 121 (1999) 2321.
[19] H. Kitagawa, N. Onodera, T. Sonoyama, M. Yamamoto, T. Fukawa, T. Mitani, M. Seto, Y. Maeda, J. Am. Chem. Soc. 121 (1999) 10068.
[20] H. Kitagawa, T. Mitani, Coord. Chem. Rev. 190–192 (1999) 1169.
[21] M. Mitsumi, T. Murase, H. Kishida, T. Yishinari, Y. Ozawa, K. Toriumi, T. Sonoyama, H. Kitagawa, T. Mitani, J. Am. Chem. Soc. 123 (2001) 11179.
[22] M. Mitsumi, K. Kitamura, A. Morinaga, Y. Ozawa, M. Kobayashi, K. Toriumi, Y. Iso, H. Kitagawa, T. Mitani, Angew. Chem. Int. Ed. 41 (2002) 2767.
[23] S. Ikeuchi, K. Saito, Y. Nakazawa, A. Sato, M. Mitsumi, K. Toriumi, M. Sorai, Phys. Rev. B66 (2002) 115110.
[24] S. Ikeuchi, K. Saito, Y. Nakazawa, M. Mitsumi, K. Toriumi, M. Sorai, J. Phys. Chem. B108 (2004) 387.
[25] H. Kitagawa, T. Sonoyama, T. Mitani, M. Seto, Y. Maeda, Synth. Met. 103 (1999) 2159.
[26] A. Kobayashi, H. Kitagawa, R. Ikeda, S. Kitao, M. Seto, M. Mitsumi, K. Toriumi, Synth. Met. 135–136 (2003) 405.
[27] M. Mitsumi, S. Umebayashi, T. Ozawa, K. Toriumi, H. Kitagawa, T. Mitani, Chem. Lett. (2002) 258.
[28] H. Tanaka, S. Kuroda, T. Yamashita, M. Mitsumi, K. Toriumi, J. Phys. Soc. Jpn. 72 (2003) 2169.
[29] H. Ito, Y. Hasegawa, H. Tanaka, S. Kuroda, M. Mitsumi, K. Toriumi, J. Phys. Soc. Jpn. 72 (2003) 2149.
[30] K. Saito, S. Ikeuchi, Y. Nakazawa, A. Sato, M. Mitsumi, T. Yamashita, K. Toriumi, M. Sorai, J. Phys. Chem. B 109 (2005) 2956.
[31] H. Matsuzaki, T. Matsuoka, H. Kishida, H. Miyasaka, K. Sugiura, M. Yamashita, H. Okamoto, Phys. Rev. Lett. 90 (2003) 046401.
[32] H. Matsuzaki, H. Kishida, H. Okamoto, K. Takizawa, S. Matsunaga, S. Takaishi, H. Miyasaka, K. Sugiura, M. Yamashita, Angew. Chem. Int. Ed. 44 (2005) 3240.
[33] M. Kuwabara, K. Yonemitsu, J. Phys. Chem. Solids 62 (2001) 247.
[34] M. Kuwabara, K. Yonemitsu, J. Mater. Chem. 11 (2001) 2163.
[35] S. Koshihara, Y. Tokura, K. Takeda, T. Koda, Phys. Rev. Lett. 68 (1992) 1148.
[36] S. Koshihara, Y. Tokura, T. Mitani, G. Saito, T. Koda, Phys. Rev. B 42 (1990) 6853;
S. Iwai, S. Tanaka, K. Fujinuma, H. Kishida, H. Okamoto, Y. Tokura, Phys. Rev. Lett. 88 (2002) 057402.
[37] C.E. Buss, K.R. Mann, J. Am. Chem. Soc. 124 (2002) 1031.
[38] M. Kato, A. Omura, A. Toshikawa, S. Kishi, Y. Sugimoto, Angew. Chem. Int. Ed. 41 (2002) 3183.
[39] Y. Wakabayashi, A. Kobayashi, H. Sawa, H. Ohsumi, N. Ikeda, H. Kitagawa, J. Am. Chem. Soc., in press.